Surface & Coatings Technology 213 (2012) 90–97

Contents lists available at SciVerse ScienceDirect

Surface & Coatings Technology

journal homepage: www.elsevier.com/locate/surfcoat

Template synthesis of raspberry-like polystyrene/SiO_2 composite microspheres and their application in wettability gradient surfaces

Xin Fan, Lianfu Zheng, Jiang Cheng *, Shouping Xu, Xiufang Wen, Zhiqi Cai, Pihui Pi, Zhuoru Yang

School of Chemistry and Chemical Engineering, South China University of Technology, Guangzhou 510640, China

ARTICLE INFO

Article history:
Received 29 June 2012
Accepted in revised form 11 October 2012
Available online 22 October 2012

Keywords:
Raspberry-like
Composite microsphere
Sol–gel
Wettability gradient
Thermal gradient field

ABSTRACT

A method to fabricate wettability gradient surface with raspberry-like composite microspheres was described. The synthesis of composite microspheres was through the ethanol sol–gel processing of TEOS on carboxyl functionalized polystyrene (PS) template particles. The factors influencing the raspberry-like morphology and the deposition efficiency of SiO_2 onto templates were discussed, including the surface carboxyl density, TEOS amount and water amount, and the optimal formulation of synthesis was given. The wettability gradient surface was built up by coating the suspension prepared on substrate and putting it in thermal gradient field for heat treatment. The resultant surface demonstrated wettability gradient from hydrophobic to superhydrophilic with the increasing of calcination temperature, which was because the physical topography of surface changed gradually from spike-type into pore-type and the main chemical compositions changed from polystyrene into SiO_2.

1. Introduction

The raspberry-like composite microspheres and relevant porous hollow capsules have attracted lots of attention in recent years for their unique properties in superhydrophobic coatings [1–4], mesoporous materials [5], targeted delivery [6] and anti-reflective film [7]. A number of routes have been developed to synthesize microspheres of this type, including Pickering (mini)emulsion polymerization [8–10], layer-by-layer assembly [11,12] and colloidal particle template synthesis [13–15]. Among these methods the template synthesis is a comparatively simple and effective approach as the size and surface reactivity of template are both controllable through the preparation of colloidal particles [5]. The sol–gel process of alkoxysilane precursors is generally used to introduce SiO_2 component onto the template surface, and it has been found that in the alkali-catalyzed sol–gel template synthesis, the positively charged or hydroxyl functionalized colloidal particles ($-NH_2$, $-OH$) always contribute to the formation of intact core–shell structure while the negatively charged ones ($-COOH$, $-SO_3H$) could lead to the generation of raspberry-like morphology [16–18]. The reason is that the anionic groups could suppress the deposition of SiO_2 on the template surface, thus hinder the formation of intact shell. Unfortunately this may also result in the phenomenon that the SiO_2 deposition efficiency on templates is rather low and a large number of free inorganic particles will self-nucleate and scatter in the final suspensions, which is unfavorable in the preparation. However in this article this so-called disadvantage would be utilized and the free SiO_2 particles would play an important role in the fabrication of wettability gradient surfaces.

Wettability gradient surface generally refers to surface with gradually varied surface energy along one dimension, which has numerous potential applications in fields of microfluidics, biomedical research and enhanced heat transfer [19–22]. The gradient effect is mainly achieved through the gradual change of either chemical composition or geometrical microstructure of the surface in the ways of UV irradiation, chemical etching, controlled deposition or contact printing [23–28], and among them thermal gradient field has been proved to be a simple and effective route for the polymer-type substrates. For example, Zhang et al. [29] utilized the melting of polystyrene (PS) microsphere under different temperatures to control the surface topography and prepared wettability gradient surface with contact angles (CAs) ranging from 148.1 to 88.7°. Similarly Lu et.al [30] fabricated surface of wetting conditions from hydrophobicity to superhydrophobicity, utilizing the porosity change of polyethylene (LDPE) film with thermal gradients. Both examples above took advantage of the physical geometrical change to tune the surface energy. Liu et.al [31] adopted another route, fabricated a chemical composition gradient from organic to inorganic by the pyrolysis of polymethylsilsesquioxane (PMSQ) with temperature and allowed wetting conditions to vary from hydrophobic to superhydrophilic.

Here in this article we attempted to fabricate wettability gradient surfaces with raspberry-like PS/SiO_2 composite microspheres and thermal gradient field. Composite microspheres would be synthesized through ethanol sol–gel processing of alkoxysilane on surface of PS template particles which were carboxylic functionalized, and factors influencing the raspberry-like morphology and SiO_2 deposition efficiency would be discussed. Then the resultant suspensions would be coated onto glass slides and calcinated in thermal gradient field, in order to

* Corresponding author. Tel./fax: +86 20 87112057.
E-mail address: cejcheng@scut.edu.cn (J. Cheng).

0257-8972/$ – see front matter © 2012 Elsevier B.V. All rights reserved.
http://dx.doi.org/10.1016/j.surfcoat.2012.10.025

fabricate wettability gradient surfaces from superhydrophobic to superhydrophilic. The relationship of wettability with calcination temperature and microspheres' raspberry-like morphology would be studied and explained.

2. Experimental

2.1. Materials

The monomers used in polymerization were all purchased in AR grade from the Lingfeng Chemical (Shanghai, China). The styrene (St) was washed with sodium hydroxide solutions (5.0 wt.%) for three times and distilled to remove the inhibitor before use. The initiator potassium persulfate (KPS) also was purchased in AR grade from the Kelong Chemical (Chengdu, China) and used after re-crystallization. The tetraethoxysilane (TEOS), dehydrated ethanol and aqueous ammonia (28.0–30.0 wt.% NH_3) were all purchased from the Guangzhou Chemical (Guangzhou, China) and used as received. DI (deionized) water was used throughout.

2.2. Synthesis of composite microspheres

The synthesis of composite microspheres was shown in Fig. 1a.

The template polymer particles were prepared via emulsifier-free emulsion polymerization with a semi-continuous feed process. At first styrene (19.33 g) and acrylic acid (0.67 g) were mixed with water (80 g) and emulsified before the solution of KPS (20 g, 0.80 wt.%) was added, afterwards the reaction was proceeded for 4 h under nitrogen at 70 °C. Then the solution of acrylic acid (AA) was added dropwise to graft carboxyl groups onto the surface of the particles and the reaction went on for another 2 h. The solution of KPS (60 g, 0.35 wt.%) was added dropwise throughout the polymerization to guarantee enough amount of radicals in the reaction system. The resultant polymer particles in emulsions were centrifugal separated, re-dispersed in ethanol and finally dried under vacuum.

Afterwards the dried template particles (0.5 g) were dispersed in dehydrated ethanol (40 g) under ultrasound before the addition of aqueous ammonia (5.0 g) and TEOS (0.25 g). Then the mixture was stirred at 50 °C in a sealed container for 10 h and aged for 24 h to make sure the completion of the sol–gel reaction. Some of resultant suspensions were centrifuged and washed with ethanol for three times, so that the composite microspheres were separated and applied to TGA, XPS, SEM and TEM analysis later.

2.3. Fabrication of wettability gradient surfaces

The resultant suspensions of sol–gel processing, which contained both composite microspheres and free SiO_2 particles, were spin coated on glass slides and annealed at 60 °C for 30 min. Then the coated specimens were heated to different temperatures ranging from 225 to 600 °C with heating speed of 10 °C/min and calcinated under that temperature for 1 h. Meanwhile a simple thermal gradient field device (Fig. 1b) was assembled with alcohol lamp and ice. As one end of the tin sheet was heated on flame and the other was put on metallic vessel full of ice water mixture, the temperature changed gradually along the length of the sheet. Then the coated glass slides were put on the tin sheet and calcinated in the thermal gradient field for 15 min, and surfaces with wettability gradient could be generated.

2.4. Characterization

The morphology of composite microspheres was observed by transmission electron microscopy (TEM, Hitachi, H-7650) and scanning electron microscopy (SEM, LEO, 1530 VP), while the surface topography of the samples after calcination was observed with scanning electron microscopy and atomic force microscopy (AFM, Being, CSPM5000). The composition of template particles and composite microspheres were studied with Fourier-transform infrared spectra (FT-IR, PerkinElmer, spectrum-2200) by dispersing the dried samples in KBr tablets. The suspensions of centrifugal separated composite microspheres were further treated with microfiltration membrane to remove free SiO_2 particles, afterwards thermogravimetric analysis (TGA, Netzsch, STA-449C-Jupiter) and X-ray photoelectron spectroscopy (XPS, Shimadzu, Kratos AXIS Ultra DLD) were used to measure the SiO_2 content in composite microspheres. The static contact angle of water on surfaces was measured with contact angle goniometer (Powereach, JC2000C1).

3. Results and discussions

3.1. FT-IR studies

Fig. 2a and b demonstrated the composition change of template particles after sol–gel processing. Compared with the spectra of PS template particles shown in Fig. 2a, there appeared absorption peak around 1100 cm^{-1} and 3400 cm^{-1} in the spectra of composite microspheres (Fig. 2b), which could be attributed to the stretching vibration of the Si–O–Si bonds and Si–OH groups generated in the sol–gel reaction of TEOS. Then the composite microspheres were

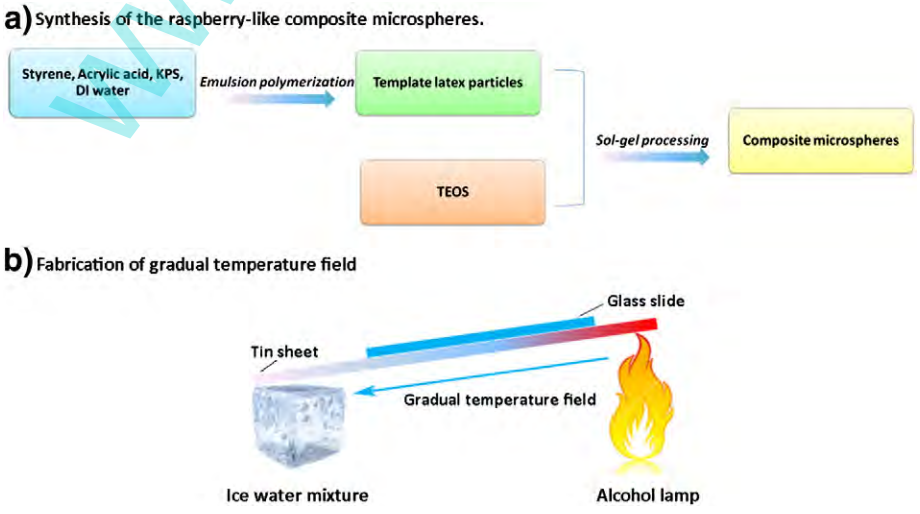

Fig. 1. Illustration of (a) synthesis of composite microspheres and (b) fabrication of wettability gradient surfaces.

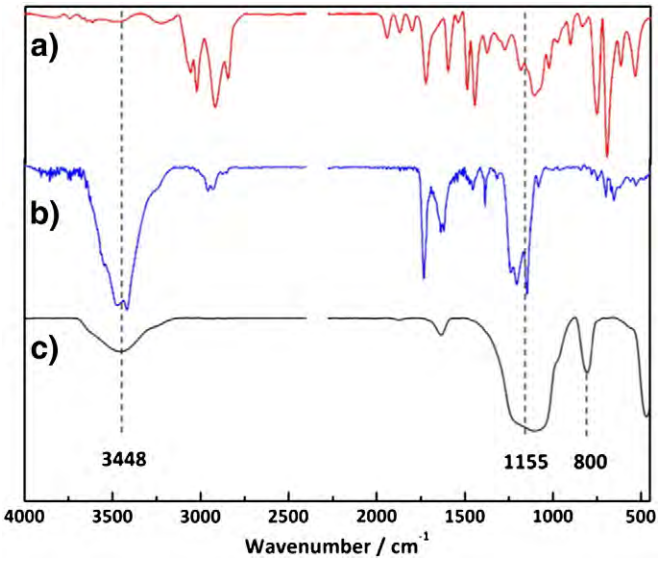

Fig. 2. FT-IR spectra of (a) PS template particles, (b) composite microspheres and (c) composite microsphere after calcination at 800 °C.

calcinated at 800 °C and the corresponding spectra were shown in Fig. 2c. It could be found that the peaks of PS templates (3027, 1597, 1504, 1446, 743, 697 cm^{-1}, phenyl group; 2923, 2819 cm^{-1}, methylene and methenyl groups) all disappeared after calcination and only peaks of silicon components left (3448, 1115 cm^{-1}, Si–O–Si bonds and Si–OH groups). Therefore we could consider that SiO_2 components were generated and it was possible to prepare composite microspheres via the sol–gel processing.

3.2. Factors influencing sol–gel processing

In order to explore the optimal formulation of preparing composite microspheres with ideal raspberry-like morphology, we designed series of experiments based on factors including surface charge density of template, TEOS amount and water amount. The summary table of recipes was shown as below (Table 1).

In the first A1–A4 series the factor of surface charge density was studied. Template particles with varied surface carboxyl densities were prepared through the adjustment of AA addition in emulsion polymerization. The *zeta* potential of the template emulsions was found to increase from −31.0 to −39.7 mV (pH = 10.0) with the change of AA amount (0–7.5 g), indicating that the surface charge density of the corresponding templates was changed as a result.

From Fig. 3 we could find that the raspberry-like morphology was better when the negative charge density of templates was lower. When AA amount was increased to 7.5 g, there were nearly no SiO_2 particles deposited on surface of template particles just as shown in Fig. 3d. This was because that the siloxane oligomers generated in the alkali-catalyzed sol–gel reaction were also negatively charged like the template particles, so the electrostatic repulsion between oligomers and templates would hinder the deposition of SiO_2 on template particle surfaces. Though there also was hydrogen-bonding attraction between silanol groups on siloxane oligomers and carboxyl groups on templates [32,33], this attraction was much weaker than the electrostatic repulsion of ionic groups. Therefore it would be difficult for siloxane oligomers to reach surface of templates when the surface negative charge density was large enough.

Table 1
Summary of experimental recipes concerning different factors.

Samples	AA amount/g	TEOS amount/g	Water amount/g
A1	***0***	0.25	0
A2	***2.5***	0.25	0
A3 (C1)	***5.0***	0.25	0
A4 (B1)	***7.5***	0.25	0
B1 (A4)	7.5	***0.25***	0
B2	7.5	***0.5***	0
B3	7.5	***1.0***	0
C1 (A3)	5.0	0.25	***0***
C2	5.0	0.25	***2.5***
C3	5.0	0.25	***10.0***

Changes of each experimental factor are highlighted in bold, italics and underline emphasis.

We could get similar conclusion from the results of XPS and TGA measurements. From the XPS spectra (Fig. 4a) we could get the quantitative data of the chemical elements on composite microsphere surface (Supplementary data, Table S-1). Then the element data were converted into the weights of compounds, and the SiO_2 contents could be calculated and compared with the TGA data as shown in the table of Fig. 4b. The XPS results were somewhat larger than the TGA ones due to the depth limit of XPS (≤100 nm), but their variation trends were the same that the SiO_2 contents decreased with the increasing of surface negative charge density.

The factor of TEOS amount was studied in the B1–B3 series. We increased the TEOS amount from 0.25 to 1.0 g based on the template of 7.5 g AA, and found that there were more SiO_2 particles deposited on template surfaces as shown in Fig. 5a. This trend also could be found in the TGA results, as the SiO_2 contents were 10.8 wt.%, 17.4 wt.% and 38.4 wt.% respectively from B1 to B3 (Supplementary data, Fig. S-2). The reason was that there were more siloxane oligomers scattering in the suspension with larger TEOS amount, which increased the probability of collision between oligomers and template particles as well as the deposition efficiency.

The factor of water amount was researched in samples C1–C3. In the presence of water there would be three reversible reactions in the sol–gel process of TEOS as shown below [34].

$$\text{Hydrolysis}: \equiv Si\text{–}OR + H_2O \leftrightharpoons \equiv Si\text{–}OH + ROH$$

$$\text{Alcohol condensation}: \equiv Si\text{–}OR + \equiv Si\text{–}OH \leftrightharpoons \equiv Si\text{–}O\text{–}Si\equiv + ROH$$

$$\text{Water condensation}: \equiv Si\text{–}OH + \equiv Si\text{–}OH \leftrightharpoons \equiv Si\text{–}O\text{–}Si\equiv + H_2O$$

When more water was added, the hydrolysis reaction of TEOS would be accelerated and more silanol groups would generate, which enhanced the hydrogen-bonding attraction between oligomers and template particles, so the deposition efficiency of SiO_2 was improved as illustrated in Fig. 5b. However if the water amount continued to increase, the reaction rate of "water condensation" would simultaneously speed up and rapidly consume silanol groups, making it more difficult to form raspberry-like microspheres. This phenomenon could also be observed in the TGA results, as the SiO_2 contents were 16.0 wt.%, 30.5 wt.% and 6.6 wt.% respectively from C1 to C3 (Supplementary data, Fig. S-3).

To sum up, with the above results we could get the optimal formulation of preparing ideal raspberry-like composite microspheres: AA amount 2.5 g, TEOS amount 1.0 g and water amount 2.5 g, and the validity of this formulation has been confirmed with experiments (Supplementary data, Fig. S-5).

3.3. Wettability change with calcination temperatures

The suspension of composite microspheres used here was prepared according to the optimal formulation above. In order to make clear the relationship of wettability with temperature, we put the coated specimens under different temperatures and measured their surface morphology and static contact angle changes. From Fig. 6 we could find that the surface topography of the film changed from spike-type (Fig. 6a) to pore-type texture (Fig. 6b and c) with

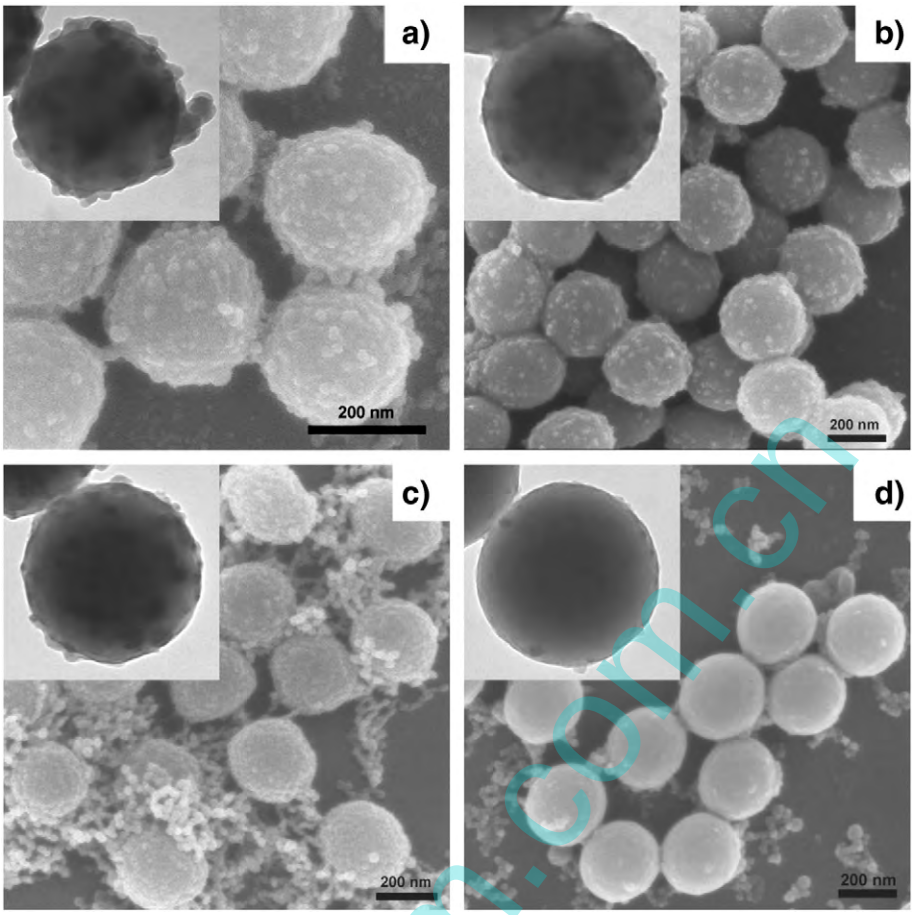

Fig. 3. SEM and TEM images of composite microspheres with AA amount of (a) 0 g, (b) 2.5 g, (c) 5 g and (d) 7.5 g.

temperature rise. In this process the bumps of composite microspheres melted and shrank gradually with the decomposition of inner PS component, and finally sacrificed to form pores. The topography changes resulted in the change of contact angles. As shown in Fig. 7 the wetting condition of samples changed from hydrophobic (CA > 110°) to superhydrophilic (CA < 3°) with the rise of calcination temperature. Combined with the TGA and DTG data of PS in air atmosphere the contact angle variation could be divided into three segments according to the calcination temperature.

I. The first temperature segment was below the decomposition temperature of PS (275 °C), in which the calcinated samples demonstrated hydrophobic property. In this segment the raspberry-like microspheres composed the main body of the surface and formed spike-type texture as shown in Figs. 6a and 8a.

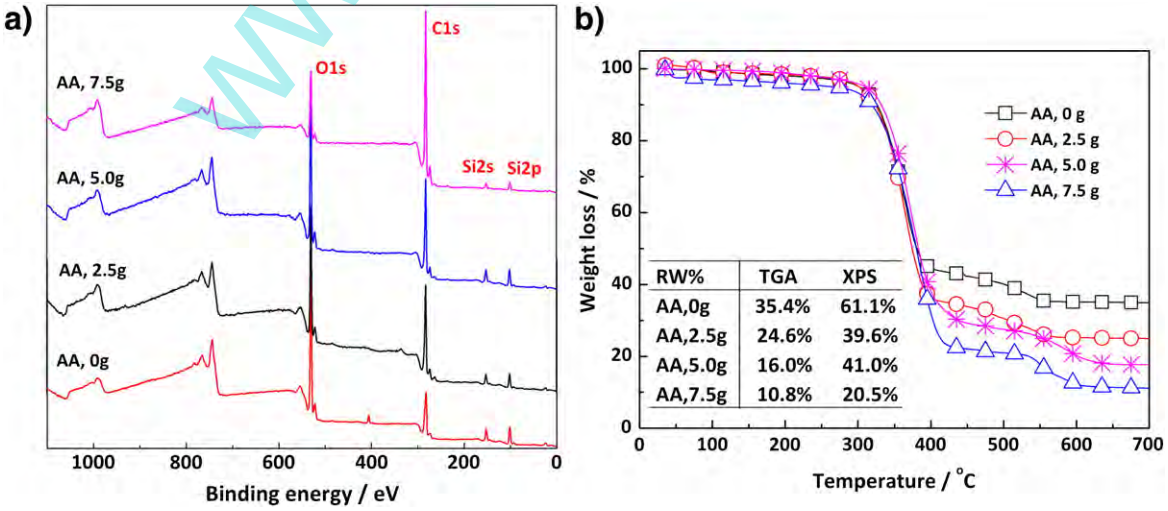

Fig. 4. (a) XPS spectra and (b) TGA results of composite microspheres with different AA amounts.

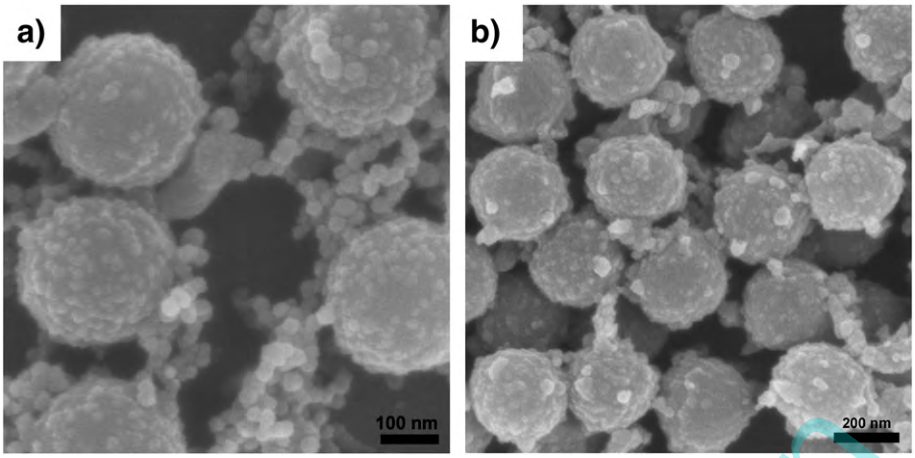

Fig. 5. SEM images of composite microspheres with (a) TEOS amount of 1.0 g and (b) water amount of 2.5 g.

The well-known Wenzel [35] or Cassie–Baxter [36] models were tried in turn to analyze the wetting ability in this situation.

In Wenzel's model water is assumed to fill up the grooves on the rough surface. Through the calculation of the surface energy change, the equilibrium condition of this model is given as:

$$\cos\theta^* = r\cdot\cos\theta_E \tag{1}$$

where θ_E is the contact angle on flat surface and r is the ratio of the real surface area to the apparent surface area.

For the surfaces in the first segment θ_E of 91° (smooth PS surface) [29], because the glass slides were spin coated with composite microspheres, the surface texture was assumed to be regular hemispherical bumps in this model. Then the maximum of the ratio r could be calculated when the microspheres were close packed:

$$r_{\max} = S_{\text{real}}/S_{\text{apparent}} = \left[(2R)^2 - \pi R^2 + \frac{1}{2}\cdot 4\pi R^2\right]/(2R)^2 = 1.785 \tag{2}$$

where R was the radius of hemispherical bumps.

Combined with Eq. (1) we could find that the maximum contact angle of the rough surface was 91.8°, which did not agree with the experimental results, so Wenzel's model was not suitable for the original state of the surface.

In the Cassie–Baxter model water does not fill up the grooves on the rough surface and air is assumed to remain trapped under the water drop, so that the drop rests on a solid/air composite surface and the hydrophobicity of surface will be improved [37]. This case could be expressed as below:

$$\cos\theta^* = \Phi_S(\cos\theta_E + 1) - 1 \tag{3}$$

where Φ_s is the relative fraction of solid phase underneath the drop. When calcination temperature was 225 °C the apparent contact angle of surface was 111.2° (Fig. 7) and the corresponding Φ_s was calculated to be $0.653<1.0$, indicating the validity of the Cassie–Baxter model in this case. Besides the dual-size surface topology of raspberry-like microspheres also is helpful for air pockets to exist between water droplet and the solid surface and reduces Φ_s, which turns the film more hydrophobic [2,4,18].

With the increasing of calcination temperature the coalescence and melting of PS component was enhanced and the roughness of surface was lowered just as shown in Fig. 8a, which resulted in the decreasing of r and increasing of Φ_s. Therefore the apparent contact angle of surface was lowered with temperature rise according to Eq. (3).

When the surface roughness decreased to certain extent the applied model might convert from Cassie–Baxter to Wenzel laws. This is because that there exists a critical value for the stability of the air-trapping regime (Cassie–Baxter model) which is given as:

$$\theta_c = \cos^{-1}[(\Phi_s - 1)/(r - \Phi_s)]. \tag{4}$$

When the contact angle θ_E is between 90° and θ_c, the air-trapping regime (Cassie–Baxter model) is metastable. Though even in this interval air is still often trapped ($\theta_c = 107.9°$ after calcination at 225 °C), the surface would finally conform to Wenzel's law and result in the further reduction of the contact angle [38].

II. The second temperature segment was between 225 and about 400 °C in which the PS decomposed. With the decomposition of polymer components the texture of hemispherical bumps gradually turned into volcano-like (Fig. 6b) and finally collapsed to form relatively flat surface. But the change of roughness was not the sole reason for the reduction of apparent contact angle. In the above process the chemical composition of surface changed from PS to SiO_2, which is much more hydrophilic ($\theta_E = 20°$) [39], so the apparent contact angle of surface was further lowered as shown in Fig. 6d. Because the flat SiO_2 surface was possible to generate when PS was half removed by calcination, the point of 50% weight loss on the TGA curve (400 °C) was selected as the upper limit of this segment.

III. The third temperature segment was the part over 400 °C. In this region the texture of surface completely changed from spike-type into pore-type texture (Fig. 6c) and the superhydrophilic phenomenon appeared. Though the film now must be porous due to the removal of PS templates on surface and inside, the water drop still could not completely spread on it (CA = 0°). This was because that the pores in the film were separated by the free SiO_2 particles and the inward permeation of water was hindered as a result.

As the hemispherical holes on surface were left after the decomposition of microsphere bumps, the maximum ratio r for this pore-type surface remained 1.785 as calculated in Eq. (2) with the assumption that the pores were close packed. Combined with the θ_E value of SiO_2 we could find that Wenzel model was not applicable in this segment as the calculated $\cos\theta^* > 1$.

The Cassie–Baxter model may be applicable in this situation. When the water drop is deposited on the surface of pore-type texture, a small amount of liquid would suck into the texture and the remaining drop would set on a solid/liquid composite surface, which is similar to the hydrophobic situation [40]. The criterion of this model is $\theta_E < \theta_c$, and θ_c is calculated according to Eq. (4). As $\Phi_s < 1$ and $r > 1$ are established fact so that θ_c must be larger than θ_E and the criterion is satisfied. From the Cassie–Baxter Eq. (3) we could find that the apparent contact angle θ^*only changed with Φ_s

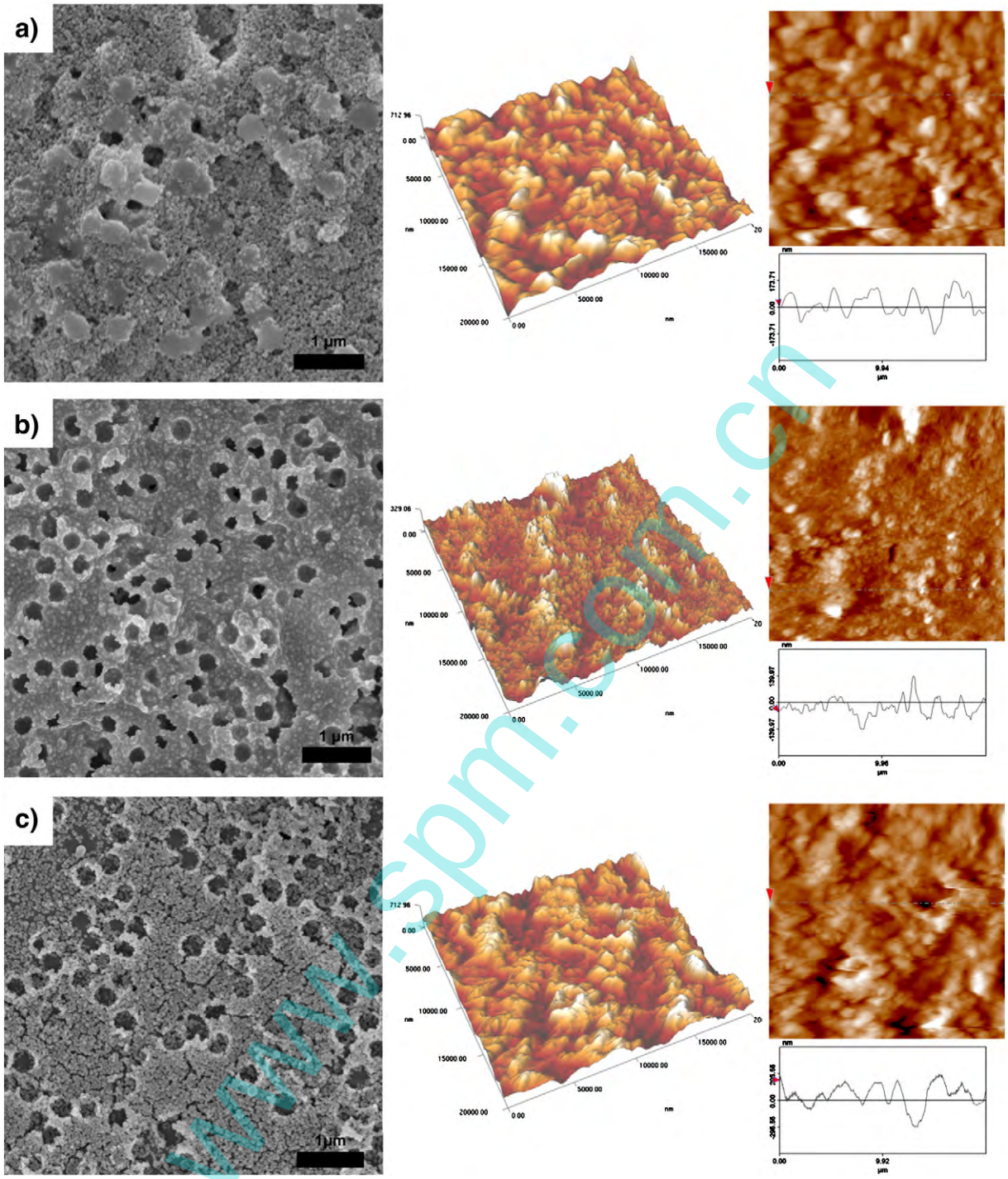

Fig. 6. SEM and AFM images of the films calcinated under (a) 225 °C, (b) 300 °C and (c) 600 °C.

on a given surface. In the temperature interval from 400 to about 475 °C there was probably still some PS component left with further decomposing, but the apparent contact angle remained constant as the Φ_s was basically fixed for the generation of pore-type surface.

Through the above analysis we could get the conclusion that the wettability of surface fabricated with the raspberry-like composite microspheres regularly changed with calcination temperature, and the range could vary from hydrophobic to superhydrophilic. Based on this finding we could build up wettability gradient surfaces of various contact angle ranges with different thermal gradient fields, just as shown in Fig. 8b.

3.4. Wettability change with raspberry-like morphology

The raspberry-like morphology of composite microsphere also was important in the wettability change, especially in the hydrophobic segment. Fig. 9 demonstrated that the contact angles of samples in segment increased with the decreasing of AA amount, i.e. the improvement of microspheres' raspberry-like morphologies.

The raspberry-like microspheres could help build up surfaces with dual-scale roughness like the self-cleaning surface of lotus leaf. The coarse-scale structure of template particles supplied the basic roughness of the hydrophobic surface, while the finer structure of SiO_2 on

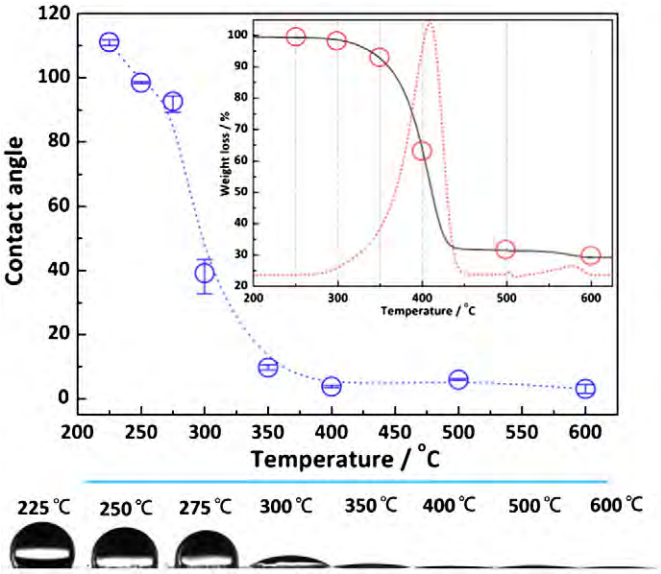

Fig. 7. Changes of contact angle with calcination temperature.

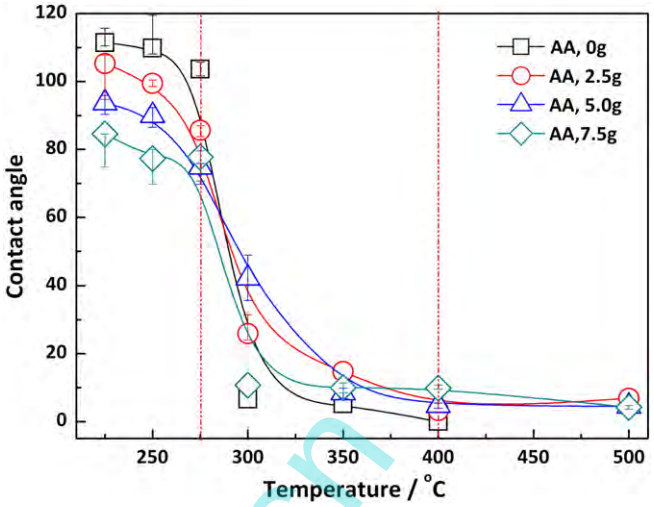

Fig. 9. Change of contact angle with calcination temperature for samples with different AA amounts.

template particles further increased the roughness and trapped more air pockets between water droplet and the solid surface. With this synergistic effect the roughness factor r in Wenzel's model (1) was increased and the solid phase fraction Φ_s in Cassie–Baxter model (3) reduced, so the surface hydrophobility was amplified [2,4,18,41–45].

From Fig. 9 it could also be found that the contact angles of samples were similar in segment II and III in which composite microspheres decomposed, further illustrating the influence of microspheres' raspberry-like morphology on the hydrophobic effect of surface.

4. Conclusions

Raspberry-like composite microspheres were synthesized through the ethanol sol–gel processing of TEOS on PS template particles. Carboxyl groups were grafted onto the PS particle surfaces to make them negatively charged, and influences of factors including surface charge density of templates, TEOS amount and water amount were discussed. It was found that the composite efficiency decreased with the increasing of AA amount due to the electrostatic repulsion effect between siloxane oligomers and templates, while the increasing of TEOS amount was helpful for the SiO_2 deposition. Addition of appropriate amount of water also was beneficial for the composite process,

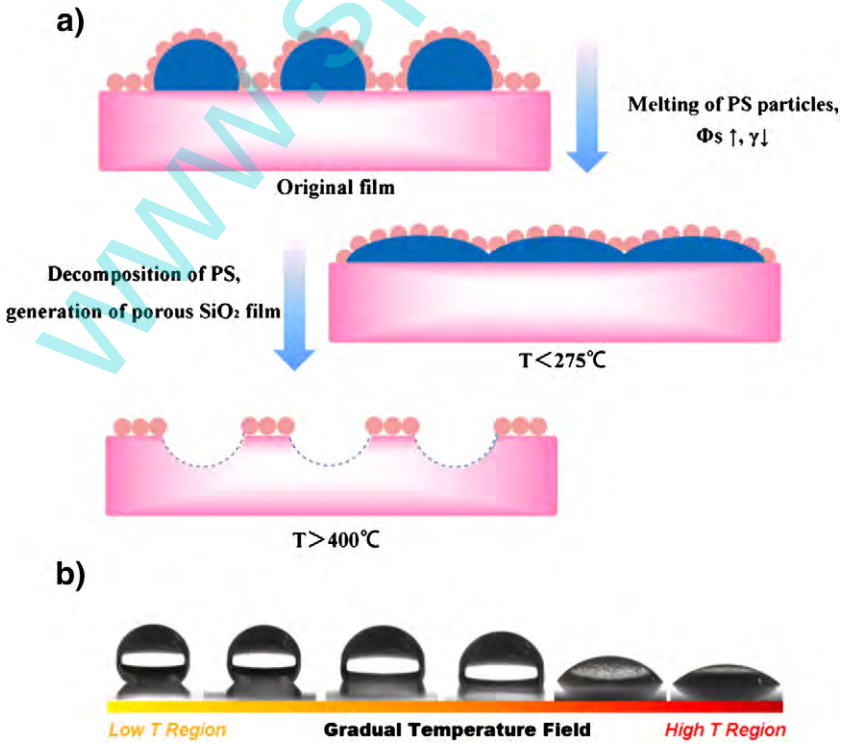

Fig. 8. (a) Geometrical structure change of surfaces with calcination temperature; and (b) Wettability gradient surface resulted from the thermal gradient field.

but excess water dosage would promote the consumption of silanol groups and hinder the formation of composite microspheres. Finally an optimal formulation was got as AA amount 2.5 g, TEOS amount 1.0 g and water amount 2.5 g,

The fabrication of wettability gradient surface was based on the physical microstructure and chemical composition changes of surface in thermal gradient field, which contained both raspberry-like composite particles and free SiO_2 particles. The surface topography changed from spike-type into pore-type due to the gradually melting and decomposition of PS templates, and the substrate composition also converted from PS onto SiO_2. Both changes resulted in a gradient wetting condition from hydrophobic to superhydrophilic, and were summarized as three temperature segments with the help of Wenzel's and Cassie–Baxter models. The relationship of the raspberry-like morphology of composite microsphere with wettability also was studied, and it was proved that raspberry-like morphology was essential in the improvement of surface hydrophobility.

Acknowledgment

It is acknowledged that this work was granted by the National Natural Science Foundation of China (no. 20976055) and the Guangdong Natural Science Foundation (no. S2012010010417).

Appendix A. Supplementary data

Supplementary data to this article can be found online at http://dx.doi.org/10.1016/j.surfcoat.2012.10.025.

References

[1] A. Qu, X. Wen, P. Pi, J. Cheng, Z. Yang, Appl. Surf. Sci. 253 (2007) 9430.
[2] H.S. Hwang, S.B. Lee, I. Park, Mater. Lett. 64 (2010) 2159.
[3] X. Du, X. Liu, H. Chen, J. He, J. Phys. Chem. C 113 (2009) 9063.
[4] W. Ming, D. Wu, R. van Benthem, G.d. With, Nano Lett. 5 (2005) 2298.
[5] X. Wu, Y. Tian, Y. Cui, L. Wei, Q. Wang, Y. Chen, J. Phys. Chem. C 111 (2007) 9704.
[6] C. Wang, J. Yan, X. Cui, H. Wang, J. Colloid Interface Sci. 354 (2011) 94.
[7] X. Li, J. He, ACS Appl. Mater. Interfaces 4 (2012) 2204.
[8] F. Tiarks, K. Landfester, M. Antonietti, Langmuir 17 (2001) 5775.
[9] Y. Zhang, H. Chen, Q. Zou, Colloid Polym. Sci. 287 (2009) 1221.
[10] A. Schrade, V. Mikhalevich, K. Landfester, U. Ziener, J. Polym. Sci., Part A: Polym. Chem. 49 (2011) 4735.
[11] F. Caruso, R.A. Caruso, H. Möhwald, Science 282 (1998) 1111.
[12] F. Caruso, H. Lichtenfeld, M. Giersig, H. Mohwald, J. Am. Chem. Soc. 120 (1998) 8523.
[13] A. Schmid, J. Tonnar, S.P. Armes, Adv. Mater. 20 (2008) 3331.
[14] S. Lee, Y.S. An, J.G. Kim, I. Park, H. Chun, G. Kim, K.H. Choi, J. Nanosci. Nanotechnol. 9 (2009) 7229.
[15] M. Chen, S. Zhou, B. You, L. Wu, Macromolecules 38 (2005) 6411.
[16] Y. Lu, J. McLellan, Y. Xia, Langmuir 20 (2004) 3464.
[17] I. Tissot, C. Novat, F. Lefebvre, E. Bourgeat-Lami, Macromolecules 34 (2001) 5737.
[18] Z. Qian, Z. Zhang, L. Song, H. Liu, J. Mater. Chem. 19 (2009) 1297.
[19] J. Cheng, Y. Zhang, P. Pi, L. Lu, Y. Tang, Int. Commun. Heat Mass Transfer 38 (2011) 1340.
[20] M.S. Kim, G. Khang, H.B. Lee, Prog. Polym. Sci. 33 (2008) 138.
[21] S. Daniel, M.K. Chaudhury, Langmuir 18 (2002) 3404.
[22] Y. Huang, X. Duan, Q. Wei, C.M. Lieber, Science 291 (2001) 630.
[23] S.H. Choi, B.Z. Newby, Langmuir 19 (2003) 7427.
[24] S.V. Roberson, A.J. Fahey, A. Sehgal, A. Karim, Appl. Surf. Sci. 200 (2002) 150.
[25] N.L. Jeon, S.K.W. Dertinger, D.T. Chiu, I.S. Choi, A.D. Stroock, G.M. Whitesides, Langmuir 16 (2000) 8311.
[26] M.B.J. Wijesundara, E. Fuoco, L. Hanley, Langmuir 17 (2001) 5721.
[27] K.M. Ashley, J. Carson Meredith, E. Amis, D. Raghavan, A. Karim, Polymer 44 (2003) 769.
[28] K. Efimenko, J. Genzer, Adv. Mater. 13 (2001) 1560.
[29] J. Zhang, L. Xue, Y. Han, Langmuir 21 (2005) 5.
[30] X. Lu, J. Zhang, C. Zhang, Y. Han, Macromol. Rapid Commun. 26 (2005) 637.
[31] H. Liu, J. Xu, Y. Li, B. Li, J. Ma, X. Zhang, Macromol. Rapid Commun. 27 (2006) 1603.
[32] H. Liu, D. Wang, X. Yang, Colloids Surf. A 397 (2012) 48.
[33] H. Zhang, X. Zhang, X. Yang, J. Colloid Interface Sci. 348 (2010) 431.
[34] R. Lindberg, J. Sjöblom, G. Sundholm, Colloids Surf. A 99 (1995) 79.
[35] R.N. Wenzel, Ind. Eng. Chem. Res. 28 (1936) 988.
[36] A.B.D. Cassie, Spec. Discuss. Faraday Soc. 3 (1948) 11.
[37] J. Bico, C. Marzolin, D. Quéré, EPL (Europhys. Lett.) 47 (1999) 220.
[38] A. Lafuma, D. Quéré, Nat. Mater. 2 (2003) 457.
[39] F.Ç. Cebeci, Z. Wu, L. Zhai, R.E. Cohen, M.F. Rubner, Langmuir 22 (2006) 2856.
[40] J. Bico, U. Thiele, D. Quéré, Colloids Surf. A 206 (2002) 41.
[41] M. Adithyavairavan, S. Subbiah, Surf. Coat. Technol. 205 (2011) 4764.
[42] H.J. Tsai, Y.L. Lee, Langmuir 23 (2007) 12687.
[43] K. Chang, Y. Chen, H. Chen, Surf. Coat. Technol. 201 (2007) 9579.
[44] Y. Bao, Q. Li, P. Xue, J. Huang, J. Wang, W. Guo, C. Wu, Mater. Res. Bull 46 (2011) 779.
[45] Y. Wang, L. Wang, S. Wang, R.J.K. Wood, Q. Xue, Surf. Coat. Technol. 206 (2012) 2258.